*Canadian Mineralogist*
Vol. 28, pp. 37-50 (1990)

# VANADIFEROUS ZINCIAN–CHROMIAN HERCYNITE IN A METAMORPHOSED BASALT-HOSTED ALTERATION ZONE, ATIK LAKE, MANITOBA

LOUIS R. BERNIER

*Department of Geological Sciences, McGill University, 3450 University Street, Montreal, Quebec H3A 2A7*

## ABSTRACT

Unusual V, Zn and Cr concentrations in hercynite (1.30–5.72 wt.% $V_2O_3$, 3.32–17.07 wt.% ZnO and 5.05–25.71 wt.% $Cr_2O_3$) are reported in a metamorphosed, tholeiitic basalt-hosted, cordierite–gedrite-bearing alteration zone associated with Fe–As–Zn–Cu–Au–Ag mineralization in the Atik Lake area, Manitoba. The grains of hercynite are very small (<25 μm) and generally subhedral. In transmitted light, they have a translucent honey-brown color and are isotropic; in reflected light, they show a low-intensity, pale grey reflectance. Single grains show relatively uniform compositions. Cr and V concentrations in the altered basalts were increased by up to 30 % as a result of mass loss due to leaching of mobile cations during hydrothermal alteration; these elements thus were relatively immobile, along with Al, Zr, Ti and Nb. The vanadiferous zincian–chromian hercynite formed during an amphibolite-facies regional metamorphism (550°C, 2.5 kbars) under low $f(O_2)$ and high $f(S_2)$ conditions.

*Keywords*: hercynite, vanadiferous, zincian, chromian, hydrothermal alteration, metamorphism, cordierite–gedrite, Atik Lake, Manitoba, electron-microprobe data, gold mineralization, arsenopyrite, löllingite, coulsonite.

## SOMMAIRE

Des concentrations anomales en V, Zn, et Cr (1.30–5.72% par poids de $V_2O_3$, 3.32–17.07 % de ZnO et 5.05–25.71% de $Cr_2O_3$) caractérisent la hercynite des roches à cordiérite–gédrite d'une zone d'altération métamorphisée dans un basalte tholéiitique, associée à une minéralisation de Fe–As–Zn–Cu–Au–Ag dans la région du lac Atik, au Manitoba. Les grains d'hercynite sont très petits (<25 μm) et généralement sub-idiomorphes. En lumière transmise, ils ont une couleur brun-miel et sont isotropes, tandis qu'en lumière réfléchie, ils ont une réflectance gris pâle. Chaque grain possède une composition relativement uniforme. Les concentrations de V et Cr dans les basaltes altérés ont augmenté jusqu'à environ 30%, par la perte de masse due au lessivage des cations mobiles, V et Cr étant particulièrement immobiles durant le processus d'altération hydrothermale, tout comme Al, Zr, Ti et Nb. La formation de l'hercynite vanadifère zincifère et chromifère est liée au métamorphisme régional dans le facies amphibolite (550°C, 2.5 kbars) sous des conditions de faible $f(O_2)$ et de $f(S_2)$ relativement élevée.

*Mots-clés*: hercynite, vanadifère, zincifère, chromifère, altération hydrothermale, métamorphisme, cordiérite–gédrite, lac Atik, Manitoba, données de microsonde électronique, minéralisation aurifère, arsenopyrite, löllingite, coulsonite.

## INTRODUCTION

Vanadiferous zincian–chromian hercynite has only rarely been reported as an accessory phase in metamorphosed hydrothermally mafic and ultramafic altered rocks, sulfide ores and associated metasediments, as well as in some unaltered ultramafic rocks (Table 1). Zincian–chromian spinel has more commonly been reported without data on the vanadium content (Table 1). This paper reports a new occurrence of such spinel in which the hercynite has the highest vanadium content ever reported. Small grains (<25 μm) of vanadiferous zincian–chromian hercynite (up to 5.72 wt.% $V_2O_3$ and up to 17 wt.% ZnO) were found in cordierite–gedrite rocks in a metamorphosed alteration pipe in the footwall basalt of an auriferous chert and associated quartz–grunerite–magnetite banded iron-formation (BIF) at Atik Lake, Manitoba.

The origin of the reported range of spinel composition is assessed through a study of bulk rock chemical changes related to premetamorphic hydrothermal alteration, and an estimate of the $P$–$T$–$f(O_2)$–$f(S_2)$ conditions of a regional episode of lower amphibolite metamorphism.

## PREVIOUS WORK

From previous work, occurrences of vanadiferous zincian–chromian spinel and zincian–chromian spinel in mafic and ultramafic rocks can be grouped into two broad categories: those in metamorphosed altered rocks associated with sulfide mineralization, and adjacent metasediments, and those in unmineralized ultramafic rocks (Table 1).

### *Mineralized areas*

Vanadiferous zincian–aluminian chromite in cordierite-bearing niccolite ores at Málaga, Spain, is considered to have crystallized from a segregated oxide liquid having unusually high V and Zn concentrations (Oen 1973). Groves *et al.* (1977) envisioned direct crystallization of zincian–aluminian chromite from a sulfide–oxide liquid enriched in Al, Ti, Cr, Zn and Mn, to explain the presence of such spinels in Fe–Ni massive sulfide ores, Western Australia.

Zoned spinel grains in mineralized ultramafic

TABLE 1. OCCURRENCES OF (VANADIFEROUS) ZINCIAN-CHROMIAN SPINEL IN MINERALIZED AREAS

| AREA | HOST ROCKS | ZNO (wt.%) | V2O3 (wt.%) | Cr/R+3 | Al/R+3 | ZONING | FACIES | ORIGIN | AUTHORS |
|---|---|---|---|---|---|---|---|---|---|
| Sykesville District Maryland. (close to ore: Fe, Cu, Zn) | Qtz-Mt chemical sediment. Metasomatized Peridotite. | 0.88-19.09 (n=20) | ----- | 0.36-0.54 | 0.00-0.52 | Intense c:Al-Zn r:Mt. | UG to LA | ME | Wylie et al. (1987) |
| Fe-Ni deposits, Western Australia. | Mineralized UM Altered peridotite. | 0.26-5.62 (n=20) | ----- | 0.54-0.90 | 0.01-0.30 | c:Zn-rich r:Mt. | A | MA ME | Groves et al. (1977) |
| Klerksdorp Goldfield, Witwatersrand, South Africa. | Detrital chromite in cglt. | 0.50-4.71 (n=8) | ----- | 0.58-0.71 | 0.20-0.43 | no zoning | LG | ME? | Utter (1978) |
| Cr-Ni-(Cu-As) mineralization, Málaga, Spain. | Crd Rocks and associated Alpine UM. | 0.60-1.00 (n=?) | 1.80-2.90 | ----- | ----- | ----- | UG LA | MA? ME | Oen (1973) |
| Cu-Co-Zn deposit, Outokumpu, Finland. | Sulfide ore and metasediments. | 0.95-14.35 0.50-12.00 (n=14) | 0.18-1.76 1.00-3.00 | 0.31-0.98 | 0.02-0.58 | c:Cr-Fe r:Zn-Al Intense | UA | ME MET | Thayer et al. (1964) Weiser (1967) Treloar (1987) Treloar et al. (1981) |
| | Crd.-Ath. rocks in stockwork zone | 0.95-26.94 (n=24) | 0.52-1.06 | 0.05-0.62 | 0.33-0.95 | | | | |
| Ni-Fe Thompson deposit, Manitoba. | Selvage between Ore and UM host rocks. | 5.00-15.00 (n=2) | ----- | 0.20-0.50 | 0.45-0.85 | ----- | UA to GR | ME ? MET? | Rimsaite & Lachance (1981) |
| Fe-As-Au-Ag-(Zn-Cu) prospects, Atik Lake, Manitoba. | Altered tholeiitic basalt (crd-ath rock) | 2.72-17.20 (n=66) | 1.03-5.72 | 0.06-0.35 | 0.57-0.92 | Weak r:Zn,Al>c | LA | ME MET | This study. |
| OCCURRENCES of (VANADIFEROUS) ZINCIAN-CHROMIAN SPINEL IN UNMINERALIZED AREAS | | | | | | | | | |
| Helgeland area, Norway | Ultramafic rocks | 0.13-2.69 (n=8) | ---- | 0.36-0.80 | 0.01-0.23 | ----- | ----- | ----- | Seelinger & Mücke (1969) Moore (1977) |
| Plan d'Albard, Italy. | Arfvedsonite-bearing Minette. | 0.06-8.74 (n=3) | ---- | 0.87 | 0.06 | ----- | ----- | MA | Wagner & Velde (1985) |
| Twin Sisters Dunite, Washington. | Alpine UM | 0.03-0.27 (n=9) | 0.11-0.21 | 0.57-0.67 | 0.20-0.39 | c:ferrit-chromite | UG | ME | Onyeagocha (1974) |

Note: UM: Ultramafic, cglt: conglomerate, Crd.-Ath.: cordierite-anthophyllite, n: number of analyses, c: core, r: rim, UG: upper greenschist, LA: lower amphibolite, A: amphibolite, UA: upper amphibolite, GR: granulite, ME: metasomatism, MA: magmatism, MET: metamorphism. -----: data not available.

rocks, Western Australia, have a zincian–aluminian chromite core and a magnetite rim, and have lower $X_{Mg}$ than chromite from layered ultramafic complexes. These zoned grains of spinel did not crystallize directly from a highly magnesian komatiitic parent magma, but have been affected by metamorphism (Groves *et al.* 1977). Complex zoning is also present in zincian chromite in metamorphosed mineralized ultramafic rocks from Sykesville, Maryland (Wylie *et al.* 1987), and in vanadiferous zincian–chromian spinel in a stockwork zone and adjacent metasediments, serpentinites and Cu–Co–Zn ores, Outokumpu, Finland (Treloar *et al.* 1981, Treloar 1987). According to Groves *et al.* (1977), the complexity of the zoning increases with metamorphic grade. It appears that in these two areas, the original chromite chemistry was modified by metasomatism either during sea-floor hydrothermal alter-

ation or during an overprinted regional metamorphic event. Treloar (1987) interpreted the high levels of Cr, V and Ni in the stockworks to result from their redistribution by hydrothermal ore-forming fluids.

Rimsaite & Lachance (1971) reported an occurence of zincian-chromian hercynite in the chloritized selvage zone between ore and ultramafic rocks at the Thompson Ni-Fe deposit, Manitoba, but did not discuss its origin.

The zincian-aluminian chromite reported in the MB5 zone below the Vaal Reef of the Klerksdorp Goldfield, Witwatersrand, was interpreted to be detrital and derived from the ultramafic rocks in the Archean greenstones (Utter 1978).

*Unmineralized areas*

Vanadiferous zincian-chromian spinel grains in unmineralized ultramafic rocks (Table 1), such as in the Helgeland area, Norway (Moore 1977), Western Australia (Groves *et al.* 1977), and Twin Sisters dunite complex (Onyeagocha 1974), usually have less than 1 wt.% ZnO and $V_2O_3$. Zinc generally is considered to be inherited from the magmatic stage, as it tends to concentrate in the silicate liquid and partition into the oxide phase (Groves *et al.* 1977). Anomalous zincian-chromian spinel (up to 8.74 wt.% ZnO) has been reported in minette at Plan D'Albard, Italy; it occurs in altered zones possibly derived from olivine, and also as inclusions in phlogopite grains (Wagner & Velde 1985). The origin of that zincian-chromian spinel is not known; the primary magmatic spinel could have been modified during a metasomatic process indicated by the presence of altered olivine.

## Analytical Technique

Electron-microprobe data were obtained with a Cameca Microbeam MB-1 instrument using wavelength dispersion. The analyses were conducted at a voltage of 15 kV, a current beam of 8 nA and counting times on standards and samples of 25 seconds. For ilmenite, V and Ti were determined using a PET (pentaerythritol) crystal and V$K\beta$ and Ti$K\alpha$ peaks, respectively, to avoid an overlap of the V$K\alpha$ and Ti$K\beta$ peaks. This problem was not encountered for the spinel grains, as the Ti concentrations are negligible. The following standards were used: kyanite (Al, Si), magnetite (Fe), willemite (Zn), diopside (Mg), $Cr_2O_3$ (Cr), spessartine (Mn), rutile (Ti), and vanadinite (V).

X-ray element mapping was done using a JEOL 100 CX TEMSCAN scanning-transmission microscope in conjunction with an energy-dispersion system (PGT System 4). An accelerating voltage of 25 kV and a current of 8 nA were used during X-ray mapping.

## Geological Setting

The Atik Lake greenstone belt is located in the Sachigo Subprovince in the Superior Province (Fig. 1) and extends for 35 km along an east-west trend with a maximum width of 10 km. A south-facing, subvertical, homoclinal sequence of volcanosedimentary units characterizes the belt. Breaks in mafic volcanism were marked by deposition of clastic and chemical sediments (BIF and auriferous chert). Periods of quiescence allowed development of hydrothermal systems (Bernier & MacLean 1989).

Small-scale alteration pipes and associated stratiform alteration developed in a tholeiitic basalt unit, footwall to a horizon of auriferous chert with related graphitic argillite and silicate-oxide BIF. Cordierite-gedrite rocks formed during the metamorphism of primary alteration assemblages in the alteration pipes. One of those pipes is well exposed; a detailed map of it (Fig. 2A) also shows the occurrences of the vanadiferous zincian-chromian hercynite.

## Mineralogy of Unaltered and Altered Basalts

The least-altered basalt is characterized by a metamorphic assemblage of hornblende and plagioclase ($An_{60}$) with a minor amount of quartz and titanite. Details on the mineralogy of the metamorphosed altered basalts and their chemistry are presented in Bernier & MacLean (1989). The metamorphism of the altered tholeiitic basalts in the pipe (Fig. 2A) led

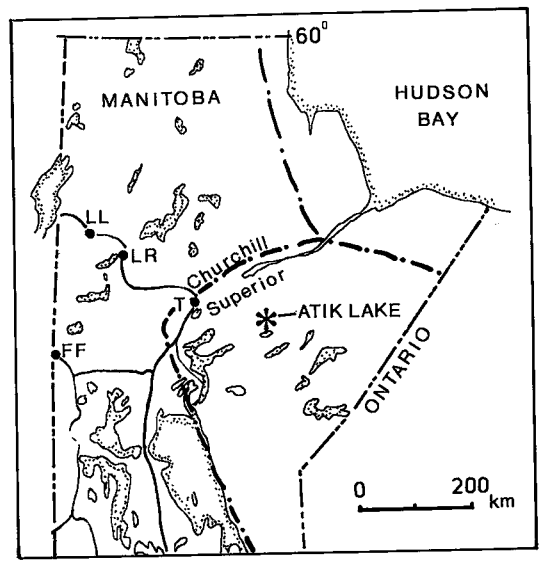


FIG. 1. Location map of the Atik Lake area, Manitoba. Symbols: FF: Flin Flon, LL:. Lynn Lake, LR: Leaf Rapids, T: Thompson.

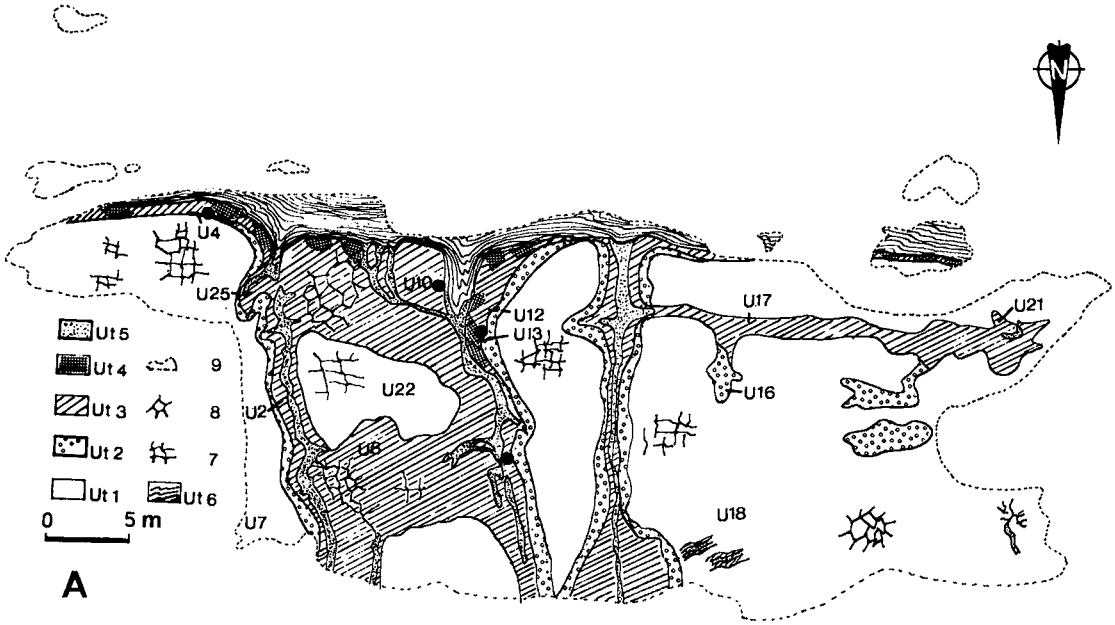


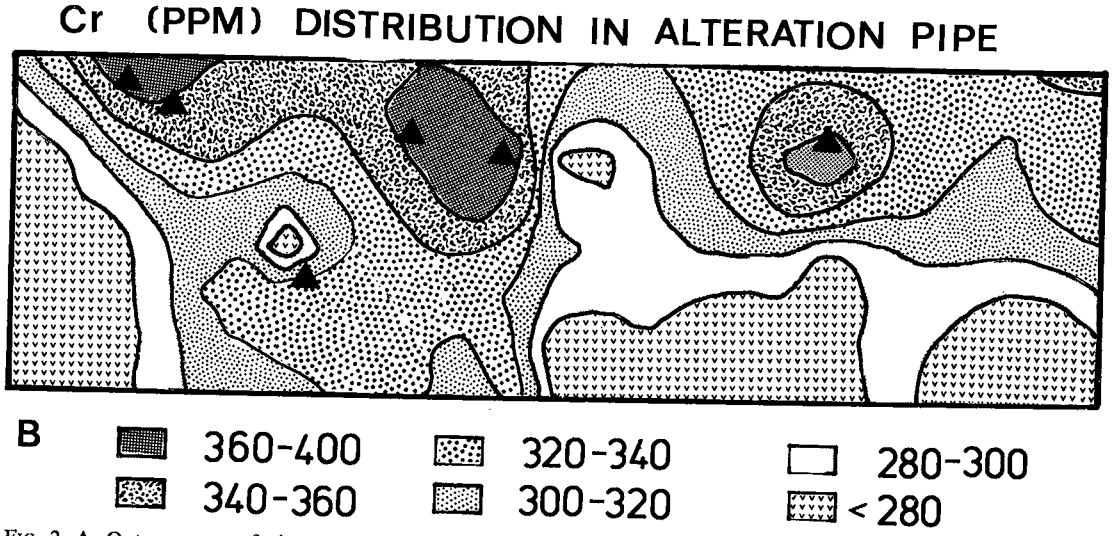


FIG. 2. A. Outcrop map of pipe 1. Symbols: Ut1: least altered glomeroporphyritic basalt, Ut2: bleached zone, Ut3: cordierite–gedrite–garnet zone, Ut4: andalusite-rich zone, Ut5: pipe conduits filled with chert and disseminated sulfides, Ut6: silicate–oxide BIF, showing deposition of BIF into the conduits, 7 and 8: fracture patterns, 9: limit of outcrop. Black dots: magnesian tourmaline. B. Contour map showing chromium concentrations in the alteration pipe. Symbols: triangles: location of samples containing vanadiferous zincian–chromian hercynite.

to the development of variable proportions of cordierite, gedrite, garnet, chlorite, biotite, andalusite, staurolite, quartz and plagioclase ($An_7$–$An_{95}$). The main oxide observed in the cordierite–gedrite rocks is a vanadiferous ilmenite (up to 1.76 wt.% $V_2O_3$: Table 2) with minor vanadiferous zincian–chromian hercynite (Table 3), rare rutile and extremely scarce magnetite rich in the coulsonite ($FeV_2O_4$) end-

TABLE 2. CHEMICAL COMPOSITIONS* OF ILMENITE AND MAGNETITE IN THE ALTERED BASALT, ATIK LAKE

| | ILMENITE | | | | | | | MAGNETITE | |
|---|---|---|---|---|---|---|---|---|---|
| (Wt.%) | U8A | U12C | U12D | U12F | U17A | U17C | U17E | U12A | U12C |
| $TiO_2$ | 51.60 | 50.79 | 51.81 | 50.70 | 50.98 | 51.27 | 51.57 | 0.82 | 0.86 |
| $Al_2O_3$ | ----- | ----- | ----- | ----- | ----- | ----- | ----- | 2.39 | 2.30 |
| $Cr_2O_3$ | 0.14 | 0.19 | 0.13 | 0.11 | 0.15 | 0.13 | 0.09 | 6.94 | 7.01 |
| $V_2O_3$* | 1.16 | 1.76 | 0.43 | 1.23 | 1.00 | 1.43 | 0.73 | 16.64 | 17.12 |
| $Fe_2O_3$ | 0.00 | 1.27 | 0.68 | 1.45 | 1.85 | 1.25 | 0.50 | 39.41 | 38.62 |
| FeO | 44.65 | 45.51 | 45.98 | 45.36 | 45.20 | 45.72 | 45.95 | 31.91 | 31.84 |
| MgO | 0.30 | 0.12 | 0.32 | 0.03 | 0.17 | 0.08 | 0.11 | ----- | ----- |
| MnO | 0.52 | 0.24 | 0.49 | 0.28 | 0.34 | 0.44 | 0.43 | 0.02 | 0.04 |
| ZnO | ----- | ----- | ----- | ----- | ----- | ----- | ----- | 0.13 | 0.10 |
| Total | 98.36 | 99.75 | 99.30 | 99.14 | 99.11 | 100.23 | 99.23 | 98.35 | 97.81 |
| $Ti_{3+}$ | 1.99 | 1.94 | 1.98 | 1.94 | 1.94 | 1.94 | 1.86 | 0.02 | 0.02 |
| $Al^{3+}$ | ----- | ----- | ----- | ----- | ----- | ----- | ----- | 0.11 | 0.10 |
| $Cr^{3+}$ | 0.00 | 0.00 | 0.00 | 0.00 | 0.00 | 0.00 | 0.00 | 0.21 | 0.21 |
| $V^{3+}$ | 0.05 | 0.07 | 0.02 | 0.05 | 0.04 | 0.06 | 0.03 | 0.51 | 0.52 |
| $Fe^{3+}$* | 0.03 | 0.05 | 0.03 | 0.05 | 0.07 | 0.05 | 0.02 | 1.13 | 1.11 |
| Fe | 1.91 | 1.93 | 1.96 | 1.93 | 1.93 | 1.93 | 1.96 | 1.02 | 1.02 |
| Mg | 0.00 | 0.00 | 0.00 | 0.00 | 0.00 | 0.00 | 0.00 | 0.00 | 0.00 |
| Mn | 0.02 | 0.01 | 0.01 | 0.01 | 0.02 | 0.02 | 0.03 | 0.00 | 0.00 |
| Total | 4.00 | 4.00 | 4.00 | 3.98 | 4.00 | 4.00 | 4.00 | 3.00 | 3.00 |

Calculations of stoichiometry made on the basis of 4 (magnetite) and 6 (ilmenite) atoms of oxygen respectively. -----:not detected. * $Fe_2O_3$ calculated from $Fe^{3+}$ determined by stoichiometry. + as determined by microprobe analyses.

member (Table 2). Traces of V and Cr (<1 wt.%) also are present in garnet and staurolite. The cordierite–gedrite rocks contain less than 5 vol.% sulfides (pyrrhotite, arsenopyrite, löllingite, chalcopyrite, sphalerite).

TABLE 3. CHEMICAL COMPOSITIONS* OF HERCYNITE IN ATIK LAKE ALTERED BASALT

| (wt.%) | U10A | U10B | U10M | U4A | U4K | U8A | U8C | U12A | U17D | U17H |
|---|---|---|---|---|---|---|---|---|---|---|
| $SiO_2$ | 0.03 | 0.09 | 0.06 | 0.03 | 0.06 | 0.13 | 0.09 | 0.07 | 0.03 | 0.06 |
| $TiO_2$ | ---- | ---- | ---- | 0.09 | 0.04 | 0.02 | 0.09 | 0.10 | 0.10 | 0.09 |
| $Al_2O_3$ | 45.84 | 31.58 | 43.69 | 44.98 | 54.44 | 41.68 | 38.43 | 38.74 | 29.95 | 33.53 |
| $Cr_2O_3$ | 13.62 | 23.87 | 14.70 | 13.43 | 5.05 | 16.18 | 16.72 | 16.13 | 25.71 | 22.42 |
| $V_2O_3$* | 1.66 | 4.54 | 1.52 | 1.58 | 1.79 | 1.30 | 5.72 | 2.66 | 2.69 | 2.02 |
| $Fe_2O_3$ | 0.00 | 2.08 | 1.07 | 0.00 | 0.00 | 1.28 | 2.00 | 4.14 | 4.36 | 3.98 |
| FeO | 27.15 | 29.26 | 28.18 | 24.98 | 19.93 | 27.06 | 29.61 | 33.61 | 32.14 | 31.01 |
| MgO | 1.38 | 0.74 | 1.62 | 1.25 | 2.05 | 1.34 | 0.75 | 0.86 | 0.51 | 0.60 |
| MnO | 0.10 | ---- | 0.10 | ---- | 0.01 | ---- | ---- | ---- | ---- | ---- |
| ZnO | 9.83 | 8.15 | 8.58 | 12.94 | 17.07 | 10.02 | 7.19 | 3.32 | 3.92 | 5.56 |
| Total | 99.51 | 98.31 | 99.52 | 99.34 | 100.44 | 99.02 | 98.80 | 99.63 | 99.41 | 99.25 |
| | Atomic Proportions (Oxygen basis 32) | | | | | | | | | |
| $Si^{4+}$ | 0.01 | 0.02 | 0.01 | 0.03 | 0.01 | 0.03 | 0.02 | 0.02 | 0.01 | 0.02 |
| $Ti^{4+}$ | ---- | ---- | ---- | 0.02 | 0.01 | 0.00 | 0.02 | 0.02 | 0.02 | 0.02 |
| $Al^{3+}$ | 13.17 | 9.74 | 12.65 | 13.05 | 15.00 | 12.26 | 11.00 | 11.45 | 9.23 | 10.20 |
| $Cr^{3+}$ | 2.63 | 4.94 | 2.86 | 2.81 | 0.93 | 3.19 | 3.39 | 3.20 | 5.32 | 4.58 |
| $V^{3+}$ | 0.30 | 0.95 | 0.30 | 0.31 | 0.34 | 0.26 | 1.18 | 0.53 | 0.56 | 0.42 |
| $Fe^{3+}$ | 0.00 | 0.41 | 0.20 | 0.00 | 0.00 | 0.24 | 0.39 | 0.78 | 0.88 | 0.77 |
| Fe | 5.54 | 6.41 | 5.79 | 5.14 | 3.90 | 5.65 | 6.35 | 7.05 | 7.03 | 6.70 |
| Mg | 0.50 | 0.29 | 0.59 | 0.46 | 0.71 | 0.50 | 0.29 | 0.32 | 0.20 | 0.23 |
| Mn | 0.02 | ---- | 0.02 | ---- | 0.00 | ---- | ---- | ---- | ---- | ---- |
| Zn | 1.77 | 1.19 | 1.58 | 2.35 | 2.95 | 1.85 | 1.38 | 0.61 | 0.76 | 1.06 |
| Total | 23.94 | 23.95 | 23.98 | 23.97 | 23.85 | 23.99 | 23.98 | 23.98 | 23.99 | 23.98 |
| | End-member Proportions | | | | | | | | | |
| Ulvo. | 0.00 | 0.00 | 0.00 | 0.25 | 0.12 | 0.00 | 0.25 | 0.25 | 0.25 | 0.25 |
| Spin. | 8.21 | 3.68 | 7.41 | 5.75 | 8.72 | 6.27 | 3.63 | 4.01 | 2.50 | 2.88 |
| Gala. | 0.25 | 0.00 | 0.25 | 0.00 | 0.00 | 0.00 | 0.00 | 0.00 | 0.00 | 0.00 |
| Chro. | 16.34 | 31.31 | 17.96 | 16.30 | 5.71 | 20.00 | 21.19 | 20.03 | 33.25 | 28.63 |
| Gahn. | 21.89 | 13.43 | 19.03 | 29.36 | 38.22 | 23.20 | 17.00 | 7.51 | 9.44 | 13.19 |
| Herc. | 53.35 | 42.97 | 52.20 | 46.41 | 47.15 | 47.40 | 48.13 | 60.01 | 45.68 | 47.63 |
| Magn. | 0.00 | 0.85 | 0.89 | 0.00 | 0.00 | 1.50 | 2.44 | 4.78 | 5.31 | 4.76 |
| Coul. | 1.88 | 6.02 | 1.88 | 1.94 | 2.09 | 1.83 | 7.38 | 3.32 | 3.50 | 2.63 |
| Fran. | 0.00 | 1.85 | 0.57 | 0.00 | 0.00 | 0.00 | 0.00 | 0.13 | 0.06 | 0.06 |

The location of the hercynite-bearing samples in the pipe is shown in Figure 2a by the first three digits of the sample number. * $Fe_2O_3$ calculated from the $Fe^{3+}$ content determined by (Al+Cr+V) deficiencies on the octahedral sites. + as determined by electron-microprobe analysis. ---- not detected. Ulvo.: ulvospinel, Spin.: spinel, Gala.: galaxite, Chro.: chromite, Gahn.: gahnite, Herc.: hercynite, Magn.: magnetite, Coul.: coulsonite, Fran.: franklinite.

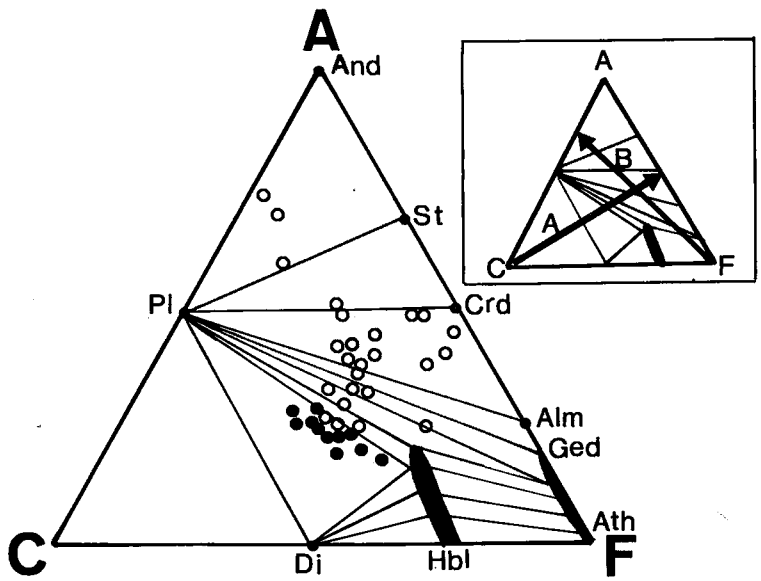


FIG. 3. Bulk-rock compositions plotted onto an ACF diagram. A: $Al_2O_3 + Fe_2O_3 - Na_2O - K_2O$, C: $CaO - 3.3\ P_2O_5$, F: FeO + MgO + MnO. Filled circle: fresh basalt, open circle: altered basalt. And: andalusite, St: staurolite, Crd: cordierite, Alm: almandine, Ged: gedrite, Ath: anthophyllite, Dio: diopside, Hbl: hornblende, Pl: plagioclase. Inset: Trend A: loss of Ca during premetamorphic hydrothermal alteration; trend B: losses of Fe+Mg during hydrothermal alteration.

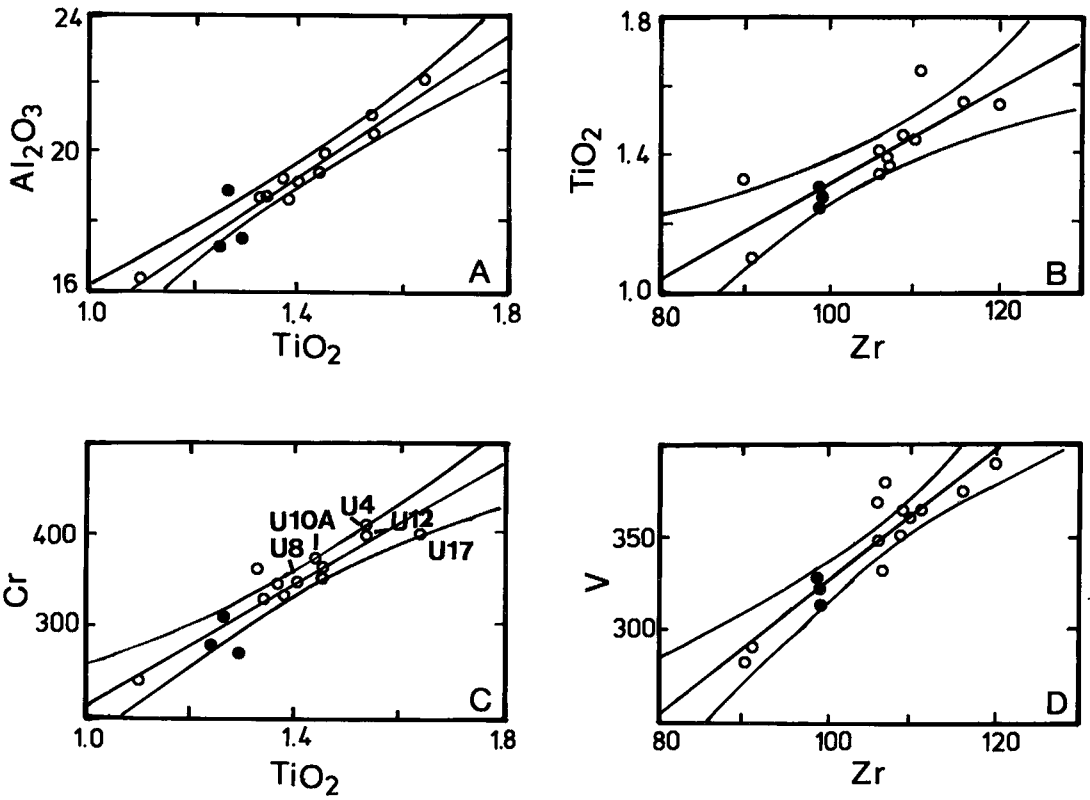


FIG. 4. Plots of element concentrations in rock from pipe 1 (major elements plotted as oxides, expressed in wt.% A. $Al_2O_3$ – $TiO_2$, B. $TiO_2$ – Zr, C. Cr – $TiO_2$ (the numbers indicate the hercynite-bearing samples of altered basalt), D. V–Zr. Solid lines through data points are derived by linear regression, and the curves reflect a 95% confidence interval. Filled circle: fresh basalt, open circle: altered basalt.

## CHEMISTRY OF UNALTERED AND ALTERED BASALTS

At Atik Lake, unaltered basalt has a tholeiitic affinity, with trace-element concentrations typical of ocean-floor basalt (Bernier & MacLean 1989). The absence of titanite in the altered rocks can be explained by a loss of Ca during hydrothermal alteration at vent sites. This loss of Ca is well depicted on an ACF diagram (Fig. 3), assuming isochemical metamorphism of the greenschist alteration-assemblages (apart from losses in volatiles). Leaching of Ca at relatively constant A–F values during alteration appears to be the main trend (A in Fig. 3). Andalusite-rich patches in the pipe (Fig. 2A) can be explained by extreme losses of Fe + Mg, as shown by trend B (Fig. 3), which terminates near the plagioclase–andalusite line. Silicification is responsible for a mass increase of up to 15% in these andalusite patches, thus inducing a dilution of the immobile elements, including Cr and V (Fig. 4). The loss of the more mobile cations, mainly Si, Ca, Na, Mg and Fe, is largely responsible for a total loss of up to 30% of the original mass (Bernier & MacLean 1989); this leaching led to enrichment in immobile components such as Al, and thus favored the appearance of assemblages of aluminous minerals during metamorphism.

TABLE 4. PEARSON CORRELATION MATRIX FOR IMMOBILE ELEMENTS IN THE PIPE

| (n=15) | $Al_2O_3$ | $TiO_2$ | Zr | V | Cr |
|---|---|---|---|---|---|
| $Al_2O_3$ | 1.00 | | | | |
| $TiO_2$ | 0.96 | 1.00 | | | |
| Zr | 0.79 | 0.84 | 1.00 | | |
| V | 0.71 | 0.77 | 0.93 | 1.00 | |
| Cr | 0.93 | 0.93 | 0.76 | 0.67 | 1.00 |

Correlation coefficients are calculated for 15 rock samples from the alteration pipe. Analyses are presented in Table 3 of Bernier & MacLean (in press).

Figures 4A to D show the effect of alteration on the behavior of the less mobile elements in the altered basalts at Atik Lake. Paired immobile elements have a high correlation-coefficient and plot along an alter-

ation trend passing through the composition of the precursor and origin, which is defined by an increase (mass loss) or a decrease (mass gain) of the immobile elements (MacLean & Kranidiotis 1987). Vanadium and chromium behaved as relatively immobile elements during the alteration of the Atik Lake basalt (Table 4, Figs. 4C, D). Additional evidence for the immobility of V and Cr comes from a study by Seyfried & Mottl (1982), who showed that V and Cr are the most immobile elements among the transition metals during experimental seawater-basalt interaction at 300°C. Furthermore, Howard & Fisk (1988) showed that an alteration crust containing aluminum-rich clays enriched in Ti, V and Cr formed by residual weathering during hydrothermal alteration of basalt on the Gorda Ridge. I have calculated a total mass-loss of up to 75% in the alteration crust from Gorda Ridge, using $Al_2O_3$ as the immobile component. This mass loss induced an increase in Cr concentration from 411 ppm in the basaltic glass to up to 1060 ppm in the alteration crust. At Atik Lake, background values of 270 ppm Cr and 315 ppm V in the least-altered tholeiite increased by a factor of up to 30% in the cordierite-gedrite rocks. The presence of vanadiferous zincian-chromian hercynite in the altered rocks is the mineralogical expression of these high-Cr and high-V zones in the alteration pipe (Figs. 2A, B). Such spinel grains have been observed only in the metamorphosed altered rocks, and no "primary" igneous chromite is found in the least-altered tholeiitic basalt. The spinel is also absent in the auriferous chert and grunerite-magnetite BIF overlying the alteration zones. The low concentrations of Cr (1–208 ppm) and V (1–128 ppm) in these chemical sediments indicate that Cr and V were not added extensively as hydrothermal components, which suggests that they were relatively immobile during hydrothermal alteration.

## Crystal-Chemistry Considerations

Spinels of the $TM_2O_4$ type have one tetrahedrally (*T*) and two octahedrally (*M*) coordinated sites; these sites can accomodate a large number of cations of different valences (2+, 3+, 4+), allowing complex solid-solutions to occur in nature (O'Neill & Navrotsky 1984). Some elements, such as Fe, V and Mn, may have more than one oxidation state, contributing to possible electron-exchange reactions. A crystal-chemistry study of natural Fe–Mg-rich chromian spinel ($0.15 \leq Cr \leq 1.07$ atoms per formula unit) by Della Giusta *et al.* (1986) shows that: Cr substitutes on both octahedral (*M*) sites, along with Al and some Mg; on the basis of strong site-preference energies, Cr only occupies octahedral (*M*) sites. Della Giusta *et al.* assigned $Si^{4+}$ exclusively to the *T* site, and $Ni^{2+}$ and $Ti^{4+}$ only to the *M* sites. The higher the Cr content, the greater the ordering of Mg in the *T* site and Al in the *M* sites. Zinc has a strong site-preference energy for tetrahedral coordination. Jacob (1976) and Bruckmann-Benke *et al.* (1988) found that the tetrahedrally coordinated site of a binary solid-solution of the type $Zn(Al,Cr)_2O_4$ is almost entirely occupied by Zn, with very small amounts of Al. Vanadium has a strong octahedral site-preference energy and is assigned (both $V^{3+}$ and $V^{4+}$) to the *M* sites (O'Neill & Navrotsky 1984).

For the Atik Lake spinel, I have assumed that all Mn is divalent and that all V is trivalent. $Fe^{3+}$ has been calculated from atomic proportions based on 32 oxygen atoms (24 cations) and was obtained as the difference between the sum of the octahedrally coordinated cations ($Al + Cr + V^{3+}$) and 16.00. End-member proportions were computed with an algorithm for which all Ti, Cr, V, Mn and Mg were used to form, respectively, ulvöspinel, chromite, coulsonite, galaxite, and spinel. Zn was combined with excess $Fe^{3+}$ after the formation of magnetite to form franklinite. Any remaining Zn was combined with Al to form gahnite, and the leftover Fe and Al were attributed to hercynite (Table 3).

Elements having a strong negative correlation (Table 5) are inferred to substitute for each other in a given site (*e.g.*, Al–Cr, Mg–Cr on the *M* sites; $Fe^{2+}$–Zn, $Fe^{2+}$–Mg on the *T* site). Those having a strong positive correlation involve *T*- and *M*-type cations (*e.g.*, Zn–Al, $Fe^{2+}$–Cr, $Fe^{2+}$–$Fe^{3+}$), a reflection of specific end-members. Treloar (1987) found negative correlations between Zn and Cr, and between Fe and Al for spinel at Outokumpu, indicating an inverse relationship between the $FeCr_2O_4$–$ZnAl_2O_4$ components.

## Characteristics of the Hercynite

### *Optical properties*

The vanadiferous zincian–chromian hercynite occurs as small subhedral grains (<25 μm) having a honey-brown to dark olive color, strong relief, and low ($R\% \approx 12$) reflectance (grey). The hercynite commonly is found close to garnet porphyroblasts, rarely as inclusions, and usually in a matrix of quartz,

TABLE 5. PEARSON CORRELATION MATRIX FOR CONCENTRATION OF CATIONS IN HERCYNITE FROM ATIK LAKE

| (n=66) | Al | Cr | V | $Fe^{3+}$ | $Fe^{2+}$ | Mg | Zn |
|---|---|---|---|---|---|---|---|
| Al | 1.00 | | | | | | |
| Cr | -0.97 | 1.00 | | | | | |
| V | -0.49 | 0.41 | 1.00 | | | | |
| $Fe^{3+}$ | -0.75 | 0.59 | 0.19 | 1.00 | | | |
| $Fe^{2+}$ | -0.87 | 0.78 | 0.42 | 0.81 | 1.00 | | |
| Mg | 0.91 | -0.85 | -0.45 | -0.76 | -0.87 | 1.00 | |
| Zn | 0.83 | -0.76 | -0.41 | -0.76 | -0.88 | 0.81 | 1.00 |

Correlation coefficients calculated by linear regression on 66 hercynite grains in cordierite-gedrite rocks in the pipe. The complete data-set is available upon request to the author. Representative hercynite compositions are shown in Table 3.

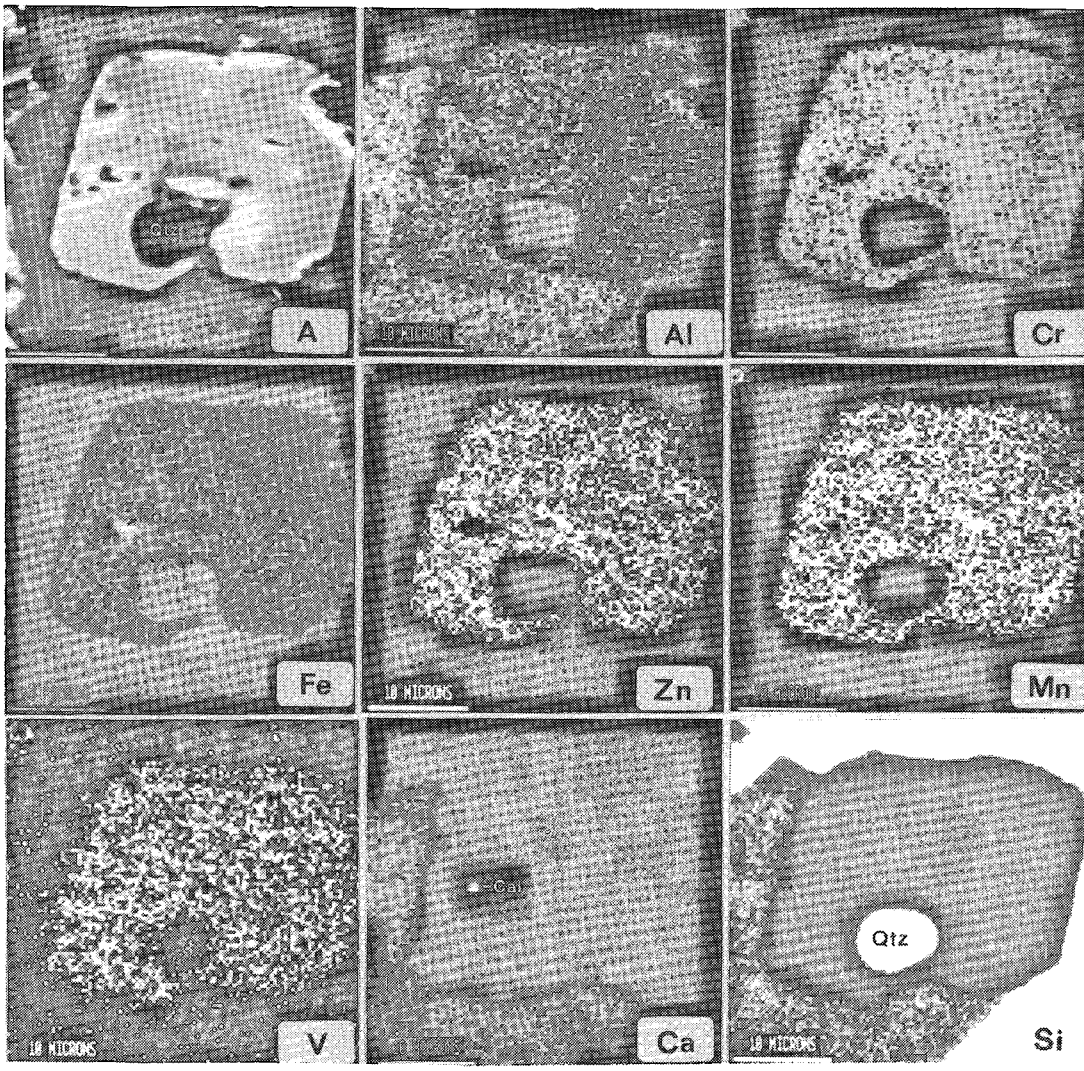


FIG. 5. SEM image of a grain of vanadiferous zincian–chromian hercynite. Others: X-ray element maps; Al, Cr, Fe [white spot corresponds to an inclusion of pyrrhotite (Po)], Zn, Mn, V, Ca (Cal: calcite inclusion beside the sulfide inclusion), Si (Qtz : large quartz inclusion in the hercynite). Bar scale: 10 $\mu$m.

plagioclase or cordierite. The hercynite grains may have micrometer-size inclusions of quartz, sulfide and carbonate (Fig. 5).

*Chemistry*

Electron-microprobe data representative of the compositional range observed are presented in Table 3. The following structural formula expresses the results of 66 microprobe analyses: $(Fe^{2+}_{0.49-0.90}Zn_{0.02-0.37}Mg_{0.02-0.09}Mn_{<0.005})(Al_{1.13-1.87}Cr_{0.12-0.69}Fe^{3+}_{0.00-0.13}V^{3+}_{0.03-0.13})O_4$.

X-ray element mapping shows that single grains of spinel are relatively homogeneous (Fig. 5), but slight increases in Al and Zn from core to rim were detected in some samples. A wide range of spinel compositions is observed within the alteration pipe (Fig. 2) and also at the thin-section scale (Figs. 6, 7). Compositional variations occur among different samples, but also in different grains in the same sample.

When compared to most other occurrences in mineralized areas, the range of spinel compositions at Atik Lake (Table 1, Fig. 6) fills a gap in previ-

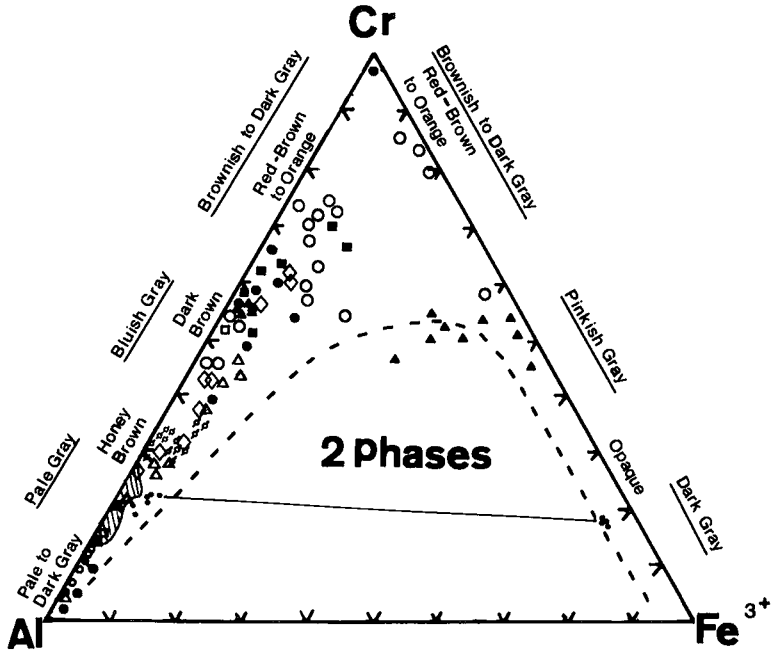


FIG. 6. Al–Cr–$Fe^{3+}$ diagram showing compositional range of (vanadiferous) zincian spinels. Optical characteristics presented on the side of the diagram are compiled from the literature; underlined is the color in reflected light; along Al–Cr and Cr–$Fe^{3+}$ sides are shown color and internal reflection in transmitted light. Dashed line: empirical miscibility gap of Loferski & Lipin (1983). Open circles: Fe–Ni deposit of Western Australia, filled triangles: Fe–Zn–Cu–Co deposits, Sykesville, Maryland, open squares: Thompson mine, Manitoba, filled squares: Klerksdorp Goldfield, Witwatersrand, filled circles: Cu–Co–Zn Outokumpu deposits, Finland. Compositions from Atik Lake: hatched field, represents 36 compositions from U10A, U4, U8, small circle with cross-line: U10B, small open circle with arrow: U17, black dots: U12. Details on location, compositions and references are given in Table 1.

ously reported data for zincian–chromian spinel. The spinel has higher $Al/R^{3+}$ ($R^{3+} = Al + Cr + V^{3+} + Fe^{3+}$) and lower $Cr/R^{3+}$ values than spinel in metamorphosed altered ultramafic rocks. This statement is also valid for compositions of spinel in ultramafic rocks in unmineralized areas (Onyeagocha 1974, Moore 1977, Wagner & Velde 1985; Table 1). A spinel from the selvage zone between Ni-ore and its ultramafic host at the Thompson mine, Manitoba (Rimsaite & Lachance 1971), falls within the compositional range observed at Atik Lake. Core compositions of spinel in the cordierite–anthophyllite rocks from the Outokumpu deposit have much higher $Cr/R^{3+}$ values than their rim, which is more aluminous and falls within the Atik Lake compositional field (Fig. 6; Treloar *et al.* 1981, Treloar 1987). Another striking characteristic of the spinel at Atik Lake is its general lack of intense compositional zoning, as was reported elsewhere for grains of zincian–chromian spinel that reach up to 700 $\mu$m across (Weiser 1967, Groves *et al.* 1977, Treloar 1987, Wylie *et al.* 1987).

A continuum of compositions in natural chromium-rich spinel exists between chromian magnetite and "ferritchromit" through $Fe^{3+}$-poor, low-aluminum chromite through chromian hercynite to pure hercynite, as discussed by Evans & Frost (1975). The zincian–chromian hercynite compositions compiled from the literature also show this continuum (Fig. 6) and plot next to an empirically determined miscibility gap, outlined by Loferski & Lipin (1983).

Interestingly, a euhedral crystal of magnetite containing ~2.5 wt. % $Al_2O_3$, ~7% $Cr_2O_3$ and ~17% $V_2O_3$ was found to coexist with the vanadiferous zincian–chromian hercynite in sample U12 (Tables 2, 3). The slightly low analytical totals for the magnetite (Table 4) could result from the presence of $V^{4+}$, as all the vanadium was taken to be $V^{3+}$ in the calculations. If this is so, the presence of $V^{4+}$ would lead to overestimation of $Fe^{3+}$ as a conse-

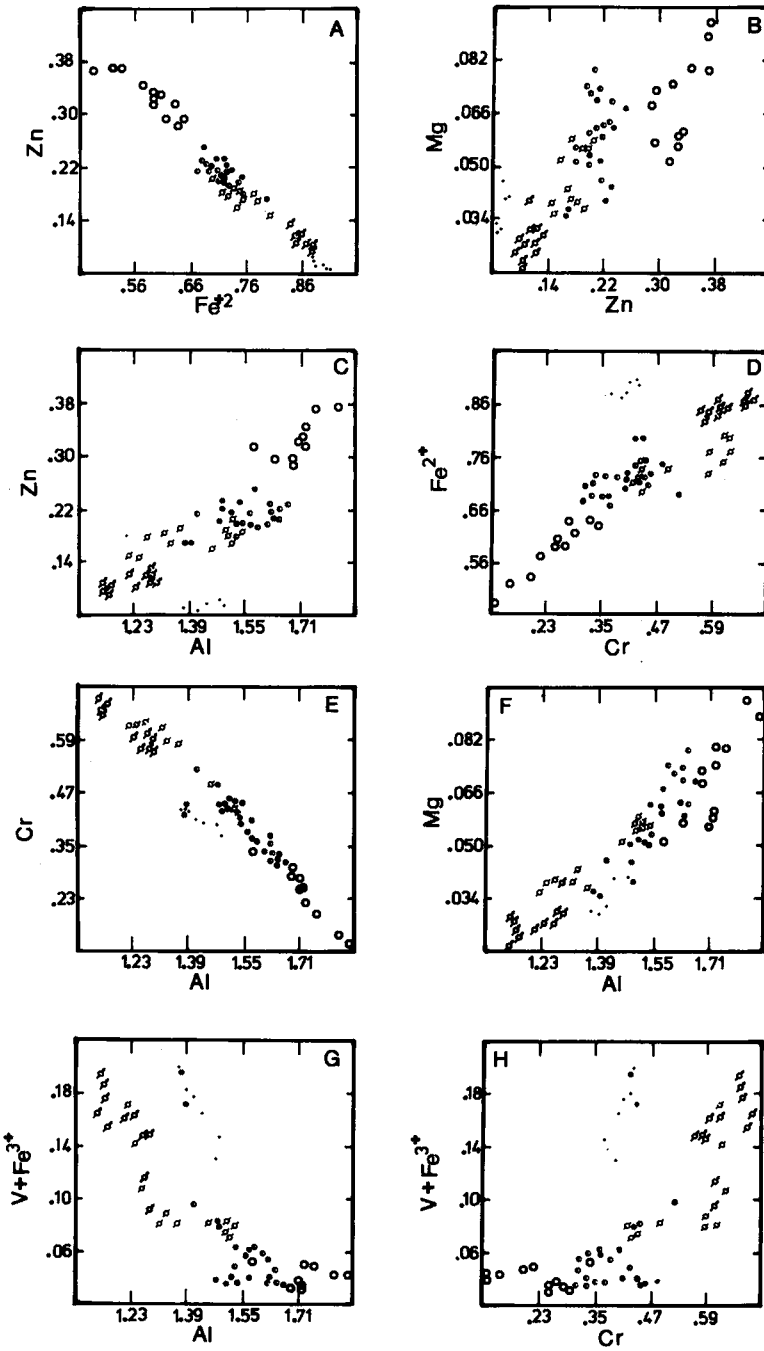


FIG. 7. Binary diagrams showing compositional ranges of hercynite from Atik Lake. Symbols: half-filled circle: U10A, small circle with cross-line: U10B, open circle: U4, filled circle: U8, small dots: U12, open circle with arrow: U17. Correlation coefficients as in Table 5. Concentrations in number of cations.

quence of an electron-exchange reaction such as $Fe^{3+} + V^{3+} = Fe^{2+} + V^{4+}$ (Wakihara *et al.* 1971).

The hercynite grains in sample U12 have high calculated concentrations of $Fe^{3+}$ (Table 3) and plot

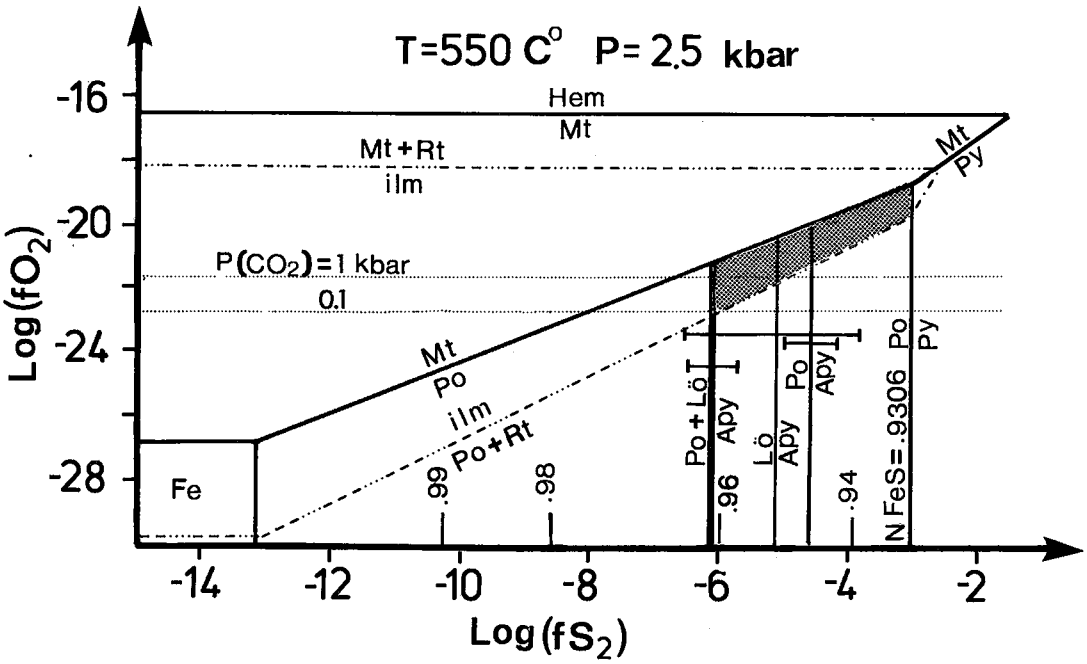


FIG. 8. Log $f(O_2)$ – log $f(S_2)$ diagram. Shaded area shows the stability field of the hercynite at Atik Lake. Symbols: Hem: hematite, Mt: magnetite, Rt: rutile, Ilm: ilmenite, Po: pyrrhotite, Py: pyrite, Lö: löllingite, Apy: arsenopyrite. $N_{FeS}^{Po}$ values shown along the log $f(S_2)$ axis calculated using equations of Froese & Gunter (1976). The error bars for the Apy and Lö boundaries are calculated using the $\Delta G_f^0$ uncertainties of Barton & Skinner (1979). Other sources of thermodynamic data as indicated in the text.

close to one limb of the proposed miscibility gap, whereas the magnetite crystals plot near the opposite limb (Fig. 6). For the vanadiferous spinel, a fourth component has to be considered; the compositional fields and tie line are projected from that fourth component onto the $Fe^{3+}$–Al–Cr plane. The effect on the solvus of adding V to the system is not known. No evidence of exsolution was found in the Atik Lake spinel. Slightly higher $f(O_2)$ conditions in this part of the alteration pipe (Fig. 2A) led to the formation of the coexisting spinel in local areas of appropriate bulk-compositions. A rare case of unmixing in primary igneous chromite (Loferski & Lipin 1983) was attributed to metamorphic re-equilibration at temperatures around 600°C. As no primary igneous spinel has been identified in the unaltered basalt at Atik Lake, a metamorphic origin for these coexisting spinels is indicated.

## CONDITIONS OF METAMORPHISM

Peak conditions of metamorphism at Atik Lake are estimated to have been $T = 550$°C and $P < 3.0$ kbars (Bernier & MacLean 1989). The pressure is not as well constrained as the temperature. The garnet–hornblende geothermometer of Graham & Powell (1984) gives core and rim temperatures of 557°C and 531°C for sample U2C within the pipe. The garnet–hornblende geobarometer of Kohn & Spear (1989) provides core and rim pressures of 3.3 and 2.8 kbars for sample U2C using the activities for the Mg end-members. The core compositions of coexisting garnet–cordierite pairs in the alteration pipe indicates maximum pressures ranging from 2.5 to 3 kbars at the condition $P = P(H_2O)$ using Figure 10 of Aranovich & Podlesskii (1983). The presence of the assemblage cordierite–chlorite–biotite–muscovite in sample U4 indicates a minimum pressure between 1 kbar if $X(H_2O) = 1$ and 2.5 kbar if $X(H_2O) = 0$ at $T = 550$°C using the mineral compositions and the thermodynamic data of Berman (1988). With these pressure considerations and in the absence of a precise estimate of the mole fraction of $H_2O$, a peak pressure of 2.5 kbars is chosen. The stability field of the vanadiferous zincian–chromian hercynite compositions can be located in $f(S_2)$–$f(O_2)$ space using buffering assemblages and the composition of pyrrhotite in spinel-bearing samples (Table 6). The different phase-boundaries plotted in a log $f(S_2)$–log $f(O_2)$ diagram (Fig. 8) were calculated using the thermodynamic data of Clark (1966), Froese & Gunter (1976), Barton & Skinner (1979), Berman & Brown (1985), Sharp *et al.* (1985) and Berman (1988). Different $f(S_2)$–$f(O_2)$ buffer assemblages observed in

TABLE 6. AVERAGE COMPOSITIONS OF HERCYNITE FROM ATIK LAKE AND $f(O_2)$-$f(S_2)$ BUFFERING ASSEMBLAGES

| Sample | (n) | $X_{Cr}$ | $X_{Al}$ | $Fe^{3+}$ | V | $X_{Zn}$ | buffering assemblages | Log $f(S_2)$* |
|---|---|---|---|---|---|---|---|---|
| U4 | (15) | 0.12 | 0.88 | 0 | 0.04 | 0.34 | apy-lo-po-ilm-rt | ----- |
| U10A | (13) | 0.18 | 0.78 | 0 | 0.04 | 0.22 | apy-lo-po-ilm | ----- |
| U10B | (12) | 0.26 | 0.70 | 0 | 0.09 | 0.17 | apy-lo-po-ilm | -4.2 |
| U8 | ( 8) | 0.21 | 0.74 | 0.02 | 0.08 | 0.21 | ilm-po-rt | ----- |
| U12 | ( 8) | 0.20 | 0.71 | 0.09 | 0.08 | 0.07 | ilm-po-mt | -3.9 |
| U17 | (12) | 0.31 | 0.61 | 0.10 | 0.05 | 0.11 | ilm-po | -3.5 |

(n) = number of hercynite grains analyzed. * calculated at T = 550°C and P = 2.5 kbar from pyrrhotite compositions $N^{Po}_{FeS}$ = 0.9421, 0.9398, 0.9352 for sample U10B, U12 and U17 respectively using equations of Froese & Gunter (1976). ----- not analyzed. apy: arsenopyrite, lo: löllingite, po: pyrrhotite, ilm: ilmenite, rt: rutile, mt: magnetite. $X_{Cr}$=Cr/(Al+Cr+V+$Fe^{3+}$), $X_{Al}$=Al/(Al+Cr+V+$Fe^{3+}$), $X_{Zn}$=Zn/(Fe+Mg+Mn+Zn).

the Atik Lake cordierite–gedrite rocks include arsenopyrite– löllingite–pyrrhotite–ilmenite ± rutile, pyrrhotite–ilmenite–rutile and pyrrhotite–ilmenite–magnetite (Table 6). The magnetite-bearing sample (U12) has a high average $X_{Cr}$ [Cr/(Cr + Al + $V^{3+}$ + $Fe^{3+}$)] and $Fe^{3+}$ content, and the lowest $X_{Zn}$ [Zn/(Fe + Mg + Mn + Zn)]. Calculated log $f(S_2)$ values based on compositions of the pyrrhotite (method of Froese & Gunter 1976) are shown in Table 6. Sample U4 has the highest $X_{Zn}$ and lowest $X_{Cr}$ values and appears to have been buffered at the lowest values of $f(S_2)$ and $f(O_2)$, represented in Figure 8 by the intersection of the arsenopyrite–löllingite–pyrrhotite and ilmenite–pyrrhotite–rutile boundaries. Samples U10A and B were buffered at a similar value of log $f(S_2)$ (= −6.2) as sample U4, but at a higher $f(O_2)$, along the arsenopyrite–löllingite–pyrrhotite boundary within the pyrrhotite–ilmenite field, as indicated by the absence of rutile. A calculated value of $X^{Po}_{FeS}$ = 0.9247 was obtained by solving reactions (1) (Froese & Gunter 1976) and (2) (Barton & Skinner 1979) by iterations, until the two equations are satisfied by a common value of $X^{Po}_{FeS}$:

(1) □S(in pyrrhotite) = $\frac{1}{2}S_2$ (in vapor)
(2) $2FeAs_2 + 2FeS + S_2 = 4FeAsS$

For reaction (2), the composition of arsenopyrite was used (37.1 As atom%) to calculate an activity $a$FeAsS = 0.8859, and $a$$FeAs_2$ was taken to be unity. The calculated value of $X^{Po}_{FeS}$ contrasts with the measured value $X^{Po}_{FeS}$ = 0.8905 in sample U10B, which leads to a value of log $f(S_2)$ = −4.12, which is 2 log units higher than that expected from the position of the arsenopyrite–löllingite–pyrrhotite boundary. Although all three minerals are observed within the same thin section, only löllingite–arsenopyrite and pyrrhotite–arsenopyrite pairs are observed in contact. If the pyrrhotite–arsenopyrite boundary is considered instead, a pyrrhotite composition of $X^{Po}_{FeS}$ = 0.8986 is calculated (3).

(3) $2FeAsS + S_2 = 2FeS + 2(As,S)$ liquid
(4) $2FeAs_2 + S_2 = 2FeAsS + 2As$

This value of $X^{Po}_{FeS}$ (0.8986) is much closer to the measured one (0.8905) in sample U10B. The löllingite–arsenopyrite boundary (4) is calculated to occur at log $f(S_2)$ = −5.30. If the maximum uncertainty of 5 kcal on $\Delta G_T$ (Barton & Skinner 1979) is applied, the boundary may occur anywhere between −6.4 and −3.9 log $f(S_2)$, a range that overlaps both reaction (2) and (3) boundaries. This suggests that the rare pyrrhotite grains (15 μm) observed in contact with arsenopyrite in sample U10B were in local equilibrium and that reactions 3 and 4 are indicative of the $f(S_2)$ condition rather than reaction 2. The estimated range of $f(O_2)$-$f(S_2)$ values under which the vanadiferous zincian–chromian hercynite formed in the cordierite–gedrite rocks in the Atik Lake alteration zone is indicated by the shaded area in Figure 8. In summary, the assemblage arsenopyrite–löllingite–pyrrhotite–ilmenite fixed the $f(S_2)$ during metamorphism, but allowed variations of up to 2.5 log units in $f(O_2)$ within the pyrrhotite–ilmenite field. The assemblage ilmenite–pyrrhotite–rutile in sample U8 does not allow a precise estimate of $f(S_2)$-$f(O_2)$, but in view of the spinel compositions, it probably has values within the field outlined in Figure 8. The spinel samples having the highest contents of chromite and magnetite components and lowest level of the gahnite component appear to be those buffered at the highest $f(S_2)$-$f(O_2)$ values. Other factors that can influence spinel compositions are: modal amount of spinel formed in the rock and bulk composition of the rock (Fig. 4C).

The $f(O_2)$-$f(S_2)$ conditions prevailing during metamorphism in the alteration pipe contrast with those in the adjacent BIF (magnetite field; Fig. 8), auriferous chert (arsenopyrite–pyrite–pyrrhotite–ilmenite; Fig. 8) and associated graphitic argillite (pyrite–pyrrhotite–graphite–rutile; Fig. 8). None of these sedimentary horizons contain vanadiferous zincian–chromian hercynite.

## Discussion and Conclusions

### *Genesis of the Atik Lake hercynite*

Vanadiferous zincian–chromian hercynite occurs in metamorphosed altered basalt (cordierite–gedrite rocks) in an alteration pipe. The alteration zone is overlain by auriferous chert and associated graphitic argillite, and by grunerite–magnetite-bearing BIF (Bernier & MacLean 1989). Primary igneous spinel has not been observed in the fresh tholeiitic basalt.

Primary igneous chromian spinel compositions from deep-sea basalts, as reported by Haggerty (1981), are generally aluminous (up to 49 wt.% $Al_2O_3$), Mg-rich (up to 19 wt.% MgO) and may be $Fe^{3+}$-rich (up to 11 wt.% $Fe_2O_3$). The reported compositions do not show even traces of vanadium

and zinc. Spinel in deep-sea basalt occurs as inclusions in plagioclase, pyroxene, olivine and glass and may show complex zoning as a result of interaction between early-formed crystals and liquid owing to a temperature decrease (Haggerty 1981). The $Cr/R^{3+}$ values found in basalt-hosted spinel are similar to those in Atik Lake metamorphosed altered basalt, and this can readily be attributed to a bulk-composition effect.

At Atik Lake, a premetamorphic stage of hydrothermal alteration enhanced Cr–V concentrations in altered basalts as a result of mass loss (Bernier & MacLean 1989). Cr and V behaved as relatively immobile elements. $Cr^{3+}$ and $V^{3+}$ can substitute for $Fe^{3+}$ and $Al^{3+}$ because of their similar ionic radius; they may have been concentrated in aluminous clays (Howard & Fisk 1988) and chlorite when these minerals formed during the hydrothermal alteration of the basalt. Concentration of Cr in sediment *via* the clay fraction is common (Burns & Burns 1975, Treloar 1987). Regional amphibolite-facies metamorphism induced breakdown of the greenschist-facies assemblages to produce cordierite–gedrite rocks. The grains of vanadiferous zincian–chromian hercynite nucleated under relatively low $f(O_2)$ and high $f(S_2)$ conditions, at sites of available Cr–V–Al–Zn released by breakdown of precursor phases. Apart from the hercynite, which contains a major concentration of Cr, traces of Cr also were found in ilmenite, garnet and staurolite, and it is an important component in magnetite, which is scarce. Vanadium was detected in ilmenite, but is a major component (coulsonite) in magnetite (Table 4). The presence of V and Cr in other minerals of the Atik Lake alteration zone reflects the bulk composition of the rocks, acquired during hydrothermal alteration. The absence of pronounced compositional zoning in these spinel grains could be due to their very small size or may indicate that efficient diffusion occurred at the peak conditions of metamorphism.

Spinel having such unusual compositions in metamorphosed mafic and ultramafic rocks can provide a useful guide for potential mineralization of the Outokumpu type (Cu–Co–Zn), Thompson type (Fe–Ni) or Atik Lake type (Fe–As–Zn–Cu–Au–Ag). Furthermore, the spinel grains are resistant to weathering and can be incorporated into the sedimentary cycle and thus provide useful regional indicators of mineralization.

## ACKNOWLEDGEMENTS

This paper represents part of the author's doctoral research at McGill University. I thank Westmin Resources Limited, Barringer–Magenta Limited and Polestar Exploration Inc. for access to their property and for research support. Drs. W.H. MacLean, S. Wood, A.M. Abdel-Rahman and R.F. Martin reviewed a preliminary draft of this manuscript. J.E. Mungall's help on the scanning electron microscope was greatly appreciated. I acknowledge the financial assistance provided by an FCAR scholarship (La Formation des Chercheurs et l'Aide à la Recherche). Research costs were partly covered by Natural Sciences and Engineering Research Council grant A7719 to Dr. W.H. MacLean. The manuscript has also benefitted from the review of two referees.

## REFERENCES

ARANOVICH, L.Y. & PODLESSKII, K.K. (1983): The cordierite–garnet–sillimanite–quartz equilibrium: experiments and applications. *In* Kinetics and Equilibrium in Mineral Reactions (S.K. Saxena, ed.). Springer-Verlag, New York.

BARTON, P.B., JR. & SKINNER, B.J. (1979): Sulfide mineral stabilities. *In* Geochemistry of Hydrothermal Ore Deposits (H. L. Barnes, ed.). John Wiley & Sons, New York.

BERMAN, R.G. (1988): Internally-consistent thermodynamic data for minerals in the system $Na_2O$–$K_2O$–CaO–MgO–FeO–$Fe_2O_3$–$Al_2O_3$–$SiO_2$–$TiO_2$–$H_2O$–$CO_2$. *J. Petrol.* **29**, 445-522.

_____ & BROWN, T. H. (1985): Heat capacity of minerals in the system $Na_2O$–$K_2O$–CaO–MgO–FeO–$Fe_2O_3$–$Al_2O_3$–$SiO_2$–$TiO_2$–$H_2O$–$CO_2$: representation, estimation and high temperature extrapolation. *Contrib. Mineral. Petrol.* **89**, 168-183.

BERNIER, L.R. & MACLEAN, W.H. (1989): Auriferous chert, banded iron-formation and related volcanogenic hydrothermal alteration, Atik Lake, Manitoba. *Can. J. Earth Sci.* **26**, 2676-2690.

BRUCKMANN-BENKE, P., CHATTERJEE, N.D. & AKSYUK, M.A. (1988): Thermodynamic properties of $Zn(Al,Cr)_2O_4$ spinels at high temperatures and pressures. *Contrib. Mineral. Petrol.* **98**, 91-96.

BURNS, V.M. & BURNS, R.G. (1975): Mineralogy of chromium. *Geochim. Cosmochim. Acta* **39**, 903-910.

CLARK, S.P., JR. (1966): High-pressure phase equilibria. *In* Handbook of Physical Constants (S.P. Clark Jr., ed.). *Geol. Soc. Am. Mem.* **97**, 345-370.

DELLA GIUSTA, A., PRINCIVALLE, F. & CARBONIN, S. (1986): Crystal chemistry of a suite of natural Cr-bearing spinels with $0.15 \leq Cr \leq 1.07$. *Neues Jahrb. Mineral. Abh.* **155**, 319-330.

EVANS, B.W. & FROST, B.R. (1975): Chrome-spinel in progressive metamorphism — a preliminary analysis. *Geochim. Cosmochim. Acta* **39**, 959-972.

FROESE, E. & GUNTER, A.E. (1976): A note on the

pyrrhotite–sulfur vapor equilibrium. *Econ. Geol.* **71**, 1589-1594.

GRAHAM, C.M. & POWELL, R. (1984): A garnet–hornblende geothermometer: calibration, testing, and application to the Pelona schist, southern California. *J. Metamorph. Geol.* **2**, 13-31.

GROVES, D.I., BARRETT, F.M., BINNS, R.A. & MCQUEEN, K.G. (1977): Spinel phases associated with metamorphosed volcanic-type iron–nickel sulfide ores from Western Australia. *Econ. Geol.* **72**, 1224-1244.

HAGGERTY, S.E. (1981): Opaque mineral oxides in terrestrial igneous rocks. *In* Oxide Minerals (D. Rumble III, ed.). *Rev. Mineral.* **3**, Hg101-299.

HOWARD, K.J. & FISK, M.R. (1988): Hydrothermal alumina-rich clays and boehmite on the Gorda Ridge. *Geochim. Cosmochim. Acta* **52**, 2269-2279.

JACOB, K.T. (1976): Gibbs free energies of formation of $ZnAl_2O_4$ and $ZnCr_2O_4$. *Thermochim. Acta* **15**, 79-87.

KOHN, M.J. & SPEAR, F.S. (1989): Empirical calibration of geobarometers for the assemblage garnet + hornblende + plagioclase + quartz. *Am. Mineral.* **74**, 77-84.

LOFERSKI, P.J. & LIPIN, B.R. (1983): Exsolution in metamorphosed chromite from the Red Lodge district, Montana. *Am. Mineral.* **68**, 777-789.

MACLEAN, W.H. & KRANIDIOTIS, P. (1987): Immobile elements as monitors of mass transfer in hydrothermal alteration: Phelps Dodge massive sulfide deposits, Matagami, Quebec. *Econ. Geol.* **82**, 951-962.

MOORE, A.C. (1977): Zinc-bearing chromite (donathite?) from Norway: a second look. *Mineral. Mag.* **41**, 351-355.

OEN, I.S. (1973): A peculiar type of Cr–Ni-mineralization; cordierite–chromite–niccolite ores of Màlaga, Spain, and their possible origin by liquid unmixing. *Econ. Geol.* **68**, 831-842.

O'NEILL, H.ST.C. & NAVROTSKY, A. (1984): Cation distributions and thermodynamic properties of binary spinel solid solutions. *Am. Mineral.* **69**, 733-753.

ONYEAGOCHA, A.C. (1974): Alteration of chromite from the Twin Sisters dunite, Washington. *Am. Mineral.* **59**, 608-612.

RIMSAITE, J. & LACHANCE, G.R. (1971): Examples of spinel–mica associations in Canadian ultrabasic rocks and in nickel deposits. *Geol. Surv. Can. Pap.* **71B**, 82-85.

SEELIGER, E. & MÜCKE, A. (1969): Donathit, ein Tetragonaler, Zn-reicher Mischkristall von Magnetit und Chromit. *Neues Jahrb. Mineral., Monatsh.*, 49-57.

SEYFRIED, W.E. & MOTTL, M.J. (1982): Hydrothermal alteration of basalt by seawater under seawater-dominated conditions. *Geochim. Cosmochim. Acta* **46**, 985-1002.

SHARP, Z.D., ESSENE, E.J. & KELLY, W.C. (1985): A re-examination of the arsenopyrite geothermometer: pressure considerations and applications to natural assemblages. *Can. Mineral.* **23**, 517-534.

THAYER, T.P, MILTON, C., DINNIN, J. & ROSE, H., JR. (1964): Zincian chromite from Outokumpu, Finland. *Am. Mineral.* **49**, 1178-1183.

TRELOAR, P.J. (1987): The Cr-minerals of Outokumpu – their chemistry and significance. *J. Petrol.* **28**, 867-886.

_____, KOISTINEN, T.J & BOWES, D.R. (1981): Metamorphic development of cordierite–amphibole rocks and mica schists in the vicinity of the Outokumpu ore deposit, Finland. *Trans. Roy. Soc. Edinb., Earth Sci.* **72**, 201-215.

UTTER, T. (1978): The origin of detrital chromites in the Klerksdorp Goldfield, Witwatersrand, South Africa. *Neues Jahrb. Mineral., Abh.* **133**, 191-209.

WAGNER, C. & VELDE, D. (1985): Mineralogy of two peralkaline, arfvedsonite-bearing minettes. A new occurrence of Zn-rich chromite. *Bull. Minéral.* **108**, 173-187.

WAKIHARA, M., SHIMIZU, Y. & KATSURA, T. (1971): Preparation and magnetic properties of the $FeV_2O_4$-$Fe_3O_4$ system. *J. Solid State Chem.* **3**, 478-483.

WEISER, T. (1967): Zink- und Vanadium-Führende Chromite von Outokumpu, Finnland. *Neues Jahrb. Mineral., Monatsh.*, 234-243.

WYLIE, A.G., CANDELA, P.A. & BURKE, T.M. (1987): Compositional zoning in unusual Zn-rich chromite from the Sykesville district of Maryland and its bearing on the origin of "ferritchromit". *Am. Mineral.* **72**, 413-422.

*Received August 29, 1989, revised manuscript accepted October 26, 1989.*